PHYSICAL REVIEW B **93**, 214101 (2016)

Interpretation of unexpected behavior of infrared absorption spectra of ScF_3 beyond the quasiharmonic approximation

Sergei Piskunov, Pjotrs A. Žguns, Dmitry Bocharov, Alexei Kuzmin, and Juris Purans*
Institute of Solid State Physics, University of Latvia, Kengaraga Street 8, LV-1063 Riga, Latvia

Aleksandr Kalinko
Universität Paderborn, Naturwissenschaftliche Fakultät, Department Chemie, Warburger Straße 100, 33098 Paderborn, Germany

Robert A. Evarestov
Saint-Petersburg State University, 7/9 Universitetskaya nab., 199034 St. Petersburg, Russia

Shehab E. Ali
Physics Department, Faculty of Science, Suez Canal University, Ismailia, Egypt

Francesco Rocca
IFN-CNR, Institute for Photonics and Nanotechnologies, Unit FBK-Photonics of Trento, Via alla Cascata 56/C, I-38123 Povo (TN), Italy
(Received 16 March 2016; revised manuscript received 27 April 2016; published 2 June 2016)

Scandium fluoride (ScF_3), having cubic ReO_3-type structure, has attracted much scientific attention due to its rather strong negative thermal expansion (NTE) in the broad temperature range from 10 to 1100 K. Here we use the results of diffraction and extended x-ray absorption fine-structure (EXAFS) spectroscopy to interpret the influence of NTE on the temperature dependence of infrared absorption spectra of ScF_3. Original infrared absorption and EXAFS experiments in a large temperature range are presented and interpreted using *ab initio* lattice dynamics simulations within and beyond quasiharmonic approximations. We demonstrate that *ab initio* electronic structure calculations, based on the linear combination of atomic orbitals method with hybrid functionals, are able to reproduce well the experimental values of lattice parameter a_0, band gap E_g, and lattice dynamics in ScF_3. However, the simulations performed within quasiharmonic approximation fail to reproduce the temperature dependence of two infrared active bands due to the F–Sc–F bending (at 220 cm^{-1}) and Sc–F stretching (at 520 cm^{-1}) modes present in the infrared absorption spectra. To overcome this problem, an approach beyond the quasiharmonic approximation is proposed: It accounts for the negative thermal expansion of the lattice and for fluorine atom displacements due to strong F vibrational motion perpendicular to the cubic axes and allows us to explain qualitatively the temperature behavior of infrared spectra of ScF_3.

DOI: 10.1103/PhysRevB.93.214101

I. INTRODUCTION

Anharmonicity of lattice dynamics is very important in relation to many observed phenomena in crystals such as thermal expansion, structural phase transitions, and soft modes in ferroelectrics [1]. In many cases, anharmonicity is quite weak up to some temperature, below which crystal lattice dynamics and properties can be described in the framework of quasiharmonic approximation (QHA). In the QHA the phonon frequencies vary due to changes in the volume of crystal with temperature or pressure [2,3]. This is the so-called implicit anharmonicity [1]. Note that the amplitude of atomic vibrations is not introduced directly into the *ab initio* QHA calculations nor into their interpretation [1].

In strongly anharmonic systems as, for example, perovskites with negative thermal expansion (NTE) and high-temperature superconductors, the so-called explicit anharmonicity effect links the phonon frequencies and interatomic forces to the amplitude of atomic vibrations, and its treatment requires us to go beyond the quasiharmonic approximation [1,4,5].

The interest towards the implicit and explicit anharmonicity effects for ReO_3-type perovskites has been recently renewed by the discovery of large negative thermal expansion (NTE) in cubic ScF_3, which was observed in a wide temperature range from 10 to 1100 K [6]. At the same time, a much less intense effect was measured in cubic ReO_3 [7,8]. At present, the great difference between these two isostructural compounds is not yet understood, but it was demonstrated in Ref. [4] that for ScF_3 the explicit anharmonic effect is very strong. Besides the NTE effect, additional interest in ScF_3 is due to a signature of quantum phase transition near its ground state [9].

ScF_3 has a cubic ReO_3-type structure with the space group $Pm\bar{3}m(221)$ and atoms occupying Wyckoff positions Sc $1a(0, 0, 0)$ and F $3d(1/2, 0, 0)$ (Fig. 1). At atmospheric pressure the cubic structure of ScF_3 survives down to at least 10 K [6]. However, opposite to the metallic ReO_3, which has a very weak NTE effect [7,10], scandium trifluoride is an insulator with the band gap larger than 7–8 eV [11]. A cubic-to-rhombohedral [space group $R\bar{3}c(167)$] phase transition occurs in ScF_3 at high pressure ($P > 0.5$ GPa at $T \sim 300$ K or $P = 0.1$–0.2 GPa at 50 K) as determined by x-ray and neutron diffraction

*purans@cfi.lu.lv

 ©2016 American Physical Society

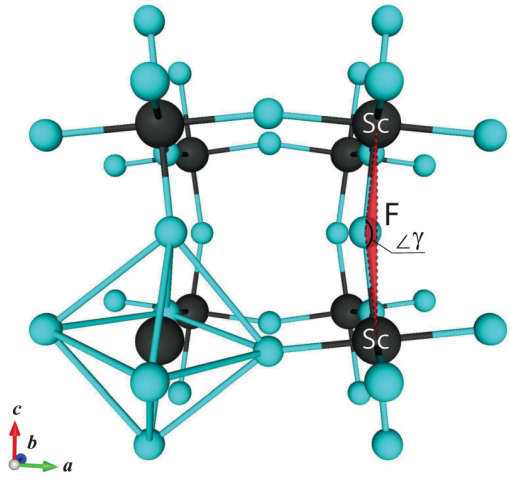

FIG. 1. Schematic view of ScF_3 structure with librated ScF_6 octahedra. The tilt angle Sc–F–Sc is defined as γ. (The small balls are fluorine atoms, the large balls are scandium atoms.)

studies [6,12]. This transition was also observed by Raman spectroscopy [12,13].

In spite of the previous experimental and theoretical efforts, the precise origin of NTE in ScF_3 is still under debate. Therefore, an additional comprehensive theoretical study is required to elucidate the nature of this effect and the role of anharmonic contributions in it.

In order to describe the NTE of ScF_3, its phonon properties were recently studied using a combination of inelastic neutron-scattering experiment with *ab initio* beyond QHA calculations of lattice dynamics [4]. It was shown that a description of NTE within the quasiharmonic approximation is not sufficient in the case of ScF_3. The authors of Ref. [4] suggested that the R^{4+} mode [the one with the lowest energy at the R point of the Brillouin zone (BZ)] responsible for the librations of the ScF_6 octahedra has quartic potential and have proposed the mechanism of NTE based on the anharmonicity consideration. The transition between the ground state and the first excited state ($\sim$19 meV) of the R^{4+} mode was associated with the experimentally observed phonon peak (at $\sim$25 meV), which stiffens as the temperature increases [4].

Another approach which can take into account implicit or explicit anharmonicity contributions is based on *ab initio* molecular dynamics (AIMD) methods. This approach, recently employed in Ref. [14] for ScF_3, allows one to compare the average lattice constants obtained from temperature-dependent isothermal-isobaric (NpT) AIMD simulations with those available from experimental data (volumetric measurements). However, the use of classical AIMD trajectories is not fully justified for simulations at low temperatures (as is the case of ScF_3 below 300 K), since the zero-phonon vibrations are not accounted for in classical AIMD [14,15]. At the same time, accurate accounting of thermal disorder effects in a wide range of temperatures may be achieved within *ab initio* quantum molecular dynamics approach [16], which is at present a challenging and computationally too intensive task.

Anharmonic effects in ScF_3 can be monitored by an analysis of the local atomic structure evaluated from the temperature-dependent extended x-ray absorption fine structure (EXAFS) measurements. EXAFS experiments allow one to measure with femtometer accuracy the average values of the instantaneous interatomic distances (bond lengths r) and the corresponding thermal expansions, whereas diffraction experiments probe the distances R (the so-called crystallographic distances) between the average positions of atoms. The bond length expansion essentially differs from the crystallographic one, due to the different influence of perpendicular vibrations [17,18].

The main results of EXAFS investigations on materials with NTE are the positive expansion of nearest-neighbor bonds and the anisotropy of atomic vibrations [8,18]. Obviously, it is hard to explain a monotonic increase of the nearest-neighbor Sc–F bonds for a static crystallographic model (space group $Pm\bar{3}m$) where the Sc–F–Sc chains remain rigid and the Sc–Sc distance (i.e., the lattice parameter) shortens [6].

In this study we describe an approach based on a simple model that goes beyond QHA for the interpretation of the unusual temperature dependence of vibrational bands in ScF_3 as shown by our new experimental infrared (IR) absorption data. We start reporting on the results of *ab initio* electronic structure and lattice dynamics calculations for ScF_3. Then the effect of anharmonicity on the NTE and on the spectroscopic properties of ScF_3 is accounted for through average fluorine atom displacements, evaluated quantitatively through the analysis of the Sc K-edge EXAFS spectra.

The paper is organized as follows. In Sec. II, the relevant details on sample preparation as well as on the IR absorption and EXAFS experiments are given. Section III describes the temperature variation of the ScF_3 structure as seen by diffraction and EXAFS. Section IV describes the method of *ab initio* calculation by linear combination of atomic orbitals (LCAO) within the framework of the hybrid density functional theory (DFT)/Hartree-Fock (HF) approach. The obtained results are presented and discussed in Sec. V within a critical comparison between QHA and beyond QHA *ab initio* modeling. Finally, the conclusions are presented in Sec. VI.

II. EXPERIMENTAL

A commercial polycrystalline ScF_3 powder (from American Elements, USA) was used in the experiments. The phase purity of the sample was checked by x-ray diffraction.

Far-infrared absorption spectra (Fig. 2) were measured using the SOLEIL synchrotron light at AILES beamline in transmission mode [19]. The spectra were recorded under vacuum in the range of 50–700 cm^{-1} using a Bruker IFS125MR Fourier transform spectrometer equipped with a bolometer. The sample temperature was controlled by a liquid helium closed-cycle cryostat in the range of 6–300 K, and the temperature was stabilized within $\pm$2 K. The sample was prepared from ScF_3 powder, which was uniformly mixed with polyethylene powder and pressed into pellets.

The EXAFS measurements were performed at the XAFS beam line of the ELETTRA Synchrotron Radiation Facility in Trieste (Italy). The EXAFS spectra at the Sc K-edge were measured in the energy range from 4200 to 6000 eV in transmission mode. A Si(111) double-crystal monochromator was used, and harmonic rejection was achieved by detuning the two crystals from the parallel alignment. The spectra were recorded

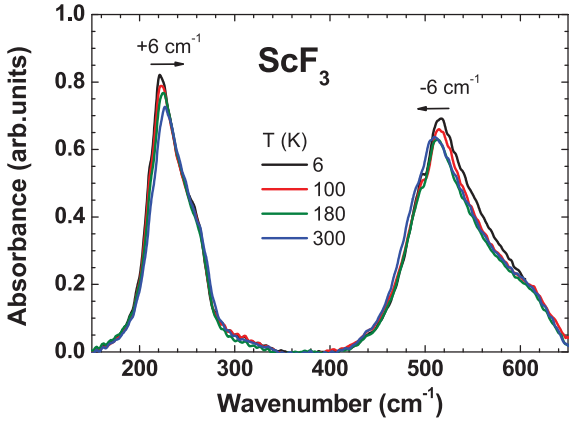

FIG. 2. Experimental infrared absorption spectra of ScF_3 at selected temperatures. Two bands related to the F–Sc–F bending (at 220 cm^{-1}) and Sc–F stretching (at 520 cm^{-1}) modes are visible. A shift of the band maxima by about 6 cm^{-1} in the opposite directions occurs on increasing temperature.

by two ionization chambers. The pre-edge and edge regions were sampled using constant energy steps, $\Delta E = 5$ and 0.5 eV, respectively, whereas the EXAFS region was sampled using constant photoelectron wave-vector step $\Delta k = 0.025$ $Å^{-1}$. The edge positions were reproducible with a precision of over 0.1 eV. At least two spectra were recorded at each temperature. Due to different sample holders for low- and high-temperature scans, we prepared the sample in two different ways: For low-temperature measurements, fine ScF_3 powder was dispersed in alcohol solution and then homogenously deposited on a polytetrafluoroethylene membrane. The sample was loaded into a helium-flow cryostat. The temperature of the sample was stabilized within ±2 K, in the whole range from 10 to 300 K. For the measurements at high temperature (in the range from 300 to 1100 K) the sample was prepared in a form of pellet containing 6 mg of fine powder of ScF_3 and 100 mg of fine powder of boron nitrate. The pellet was placed into a graphite cell mounted in a multipurpose l'Aquila-Camerino vacuum glass oven [20]. The temperature during measurements was stabilized within ±5 K. The thickness of the sample was optimized in both cases as to obtain an absorption jump $\Delta(\mu x) \simeq 1$ at the Sc K absorption edge.

III. STRUCTURAL CHANGES WITH TEMPERATURE

The structure of cubic perovskite-type ScF_3 is built up of corner-shared regular ScF_6 octahedra with Sc atoms located at the centers and linear Sc–F–Sc chains (Fig. 1). The space amid eight octahedra forming a cube is vacant, allowing for a significant tilting of the ScF_6 octahedra. As a result, the amplitude of fluorine atom thermal vibrations is anisotropic, being larger in the direction perpendicular to the Sc–F–Sc chains, while the vibrations of scandium atoms are almost isotropic [6]. The interplay between the local dynamics of the ScF_6 octahedral units and the thermal behavior of the crystal lattice is important to explain the NTE in ScF_3. Therefore, one needs to follow both effects to access the details of the NTE. Note that a small local distortion of the macroscopic cubic lattice, arising on the substitution of Sc^{3+} by isovalent cations such as Fe^{3+} or Ga^{3+}, can reduce the NTE effect resulting in zero thermal expansion [21].

A. Local atomic structure: Evaluation of distances

Precise information on the behavior of the lattice parameter of ScF_3 in the temperature range of 10 to 1100 K is available from x-ray and neutron diffraction measurements [6], whereas the local behavior of Sc–F bonds within the ScF_6 octahedra is accessible from the analysis of the Sc K-edge EXAFS spectra. The two experimental techniques provide complementary information. Diffraction is sensitive to the average atomic positions: Experiments allow one to measure the cell parameters and their temperature dependence. For crystals with atoms only in special positions, like undistorted perovskites, the distance $R = |\langle \mathbf{r}_b \rangle - \langle \mathbf{r}_a \rangle|$ between the average positions $\langle \mathbf{r}_a \rangle$ and $\langle \mathbf{r}_b \rangle$ of two atoms a and b, respectively, can be obtained from the cell parameters by direct proportionality, and its temperature variation δR is proportional to the macroscopic thermal expansion. At the same time, EXAFS experiments measure the average value of the instantaneous interatomic distances (bond lengths), $r = \langle |\mathbf{r}_b - \mathbf{r}_a| \rangle$.

The distances R and r, and the corresponding thermal expansions, differ fundamentally, due to thermal vibrations perpendicular to the direction of the interatomic bond [22,23]. The two quantities would coincide only in the case of a complete absence of any vibrations, but differ when thermal effects, including zero-point contribution, are taken into account [24,25].

The *perpendicular* mean-square relative displacements (MSRD) term $\langle \Delta u_\perp^2 \rangle$ establishes the connection between the distances measured by EXAFS and diffraction, r and R, respectively, at any temperature as [25,26]

$$r = R + \langle \Delta u_\perp^2 \rangle / 2R. \quad (1)$$

To the extent that $\langle \Delta u_\perp^2 \rangle$ increases with temperature, the thermal expansion measured by EXAFS is larger than the thermal expansion measured by diffraction. From the independent measurements of Δr and ΔR, one can obtain the behavior of the perpendicular MSRD $\langle \Delta u_\perp^2 \rangle$ by inversion of Eq. (1).

B. Results of EXAFS analysis

X-ray absorption spectra were treated using the EDA software package [27]. Since an uncertainty of a few hundredths of eV in energy definition leads to an uncertainty of a few dozens femtometers in distance differences, the edges of all spectra were carefully aligned to each other within 0.02 eV before EXAFS extraction.

The Sc K-edge EXAFS signals were extracted following the standard procedure [28,29]. The Fourier transforms (FTs) of EXAFS signals $\chi(k)k^2$ are shown in Fig. 3 at selected temperatures. The peak positions in FTs are shifted with respect to crystallographic distances because FTs were calculated without phase-shift correction. A significant decrease in the peak amplitudes when temperature increases is well visible in Fig. 3. The origin of the peaks in FTs is due to the single- and multiple-scattering effects involving the first six coordination shells around the absorbing scandium atom.

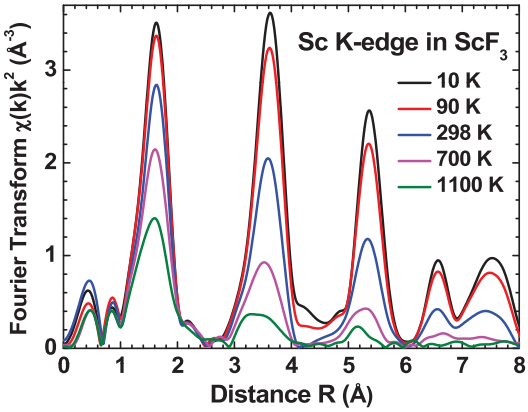

FIG. 3. Fourier transforms of the experimental Sc K-edge EXAFS $\chi(k)k^2$ for polycrystalline ScF_3 at selected temperatures from 10 to 1100 K.

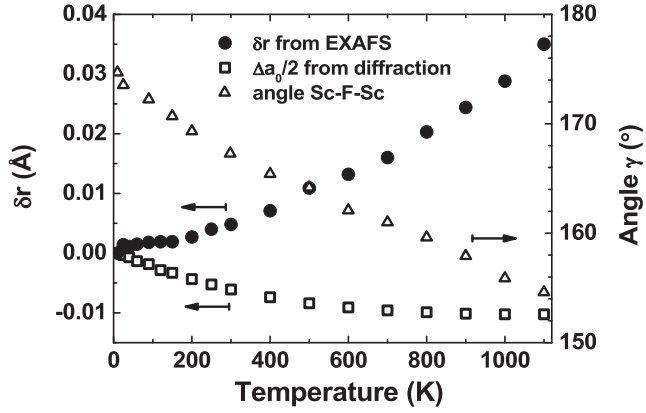

FIG. 4. Temperature dependence of the first coordination shell parameters: δr (filled circles) is the bond length Sc–F measured by EXAFS; $\Delta a_0/2$ (squares) corresponds to half of the lattice parameter obtained by diffraction in Ref. [6]; γ (triangles) is the calculated average angle Sc–F–Sc (see Fig. 1).

The first coordination shell contributions into the total EXAFS were singled out by Fourier filtering procedure within the k-space range of 0.1 to 18.0 $Å^{-1}$ and R-space range of 1.05 to 2.5 Å. They were analyzed by the best-fit procedure within the single-scattering approximation [17,29]. The backscattering amplitude and phase-shift functions were extracted from the low-temperature (10 K) EXAFS signal, therefore only differences in the interatomic distances $\delta r(T) = r(T) - r(10\text{K})$ were obtained at each temperature T and are reported in Fig. 4.

The temperature dependence of the bond length Sc–F r (values presented in Table I of Supplemental Material [30]) was evaluated from the relative values δr obtained by EXAFS (Fig. 4) as

$$r(T) = \delta r(T) + R_{T=0K} + \left\langle \Delta u_{\perp}^2 \right\rangle_{T=0K}/2R_{T=0K}, \qquad (2)$$

where $R_{T=0K} = a_0(T = 0K)/2$.

The value of $\langle \Delta u_{\perp}^2 \rangle_{T=0K} = 0.0025$ $Å^2$ was estimated from the temperature dependence of the thermal ellipsoid parameter U_{33}(F) obtained for ScF_3 by diffraction in Ref. [6]. It is related to the amplitude of zero-point vibrations at $T = 0$ K.

In summary, the experimental results of diffraction [6] and EXAFS studies indicate that, on temperature increase from 10 to 1100 K, the lattice parameter a_0 of ScF_3 contracts, whereas the first coordination shell interatomic Sc–F distance r expands. The knowledge of the lattice parameter (a_0), equal to the distance Sc–Sc, and of the average distance Sc–F (r) allowed us to calculate the average values of the tilt angle Sc–F–Sc γ (see Table I in Supplemental Material [30]), which were used in the simulations of the IR absorption spectra. Note that while the Sc–F–Sc angle evaluated for the average atomic positions is equal to 180° as observed by diffraction, it has a smaller value due to vibrations of fluorine atoms perpendicular to the direction of the Sc–F–Sc chains when calculated from mean distances obtained by EXAFS. As it is evident in Fig. 4 (triangles), this effect is clearly observed even at $T = 0$ K, when the zero-point vibrations are responsible for a little deviation of the average angle from that expected for linear coordination.

Finally, we point out that the temperature dependencies of the experimental lattice parameter [6] a_0 as well as of the obtained interatomic Sc–F distances r are well reproduced by recent AIMD simulations [14]: They show qualitatively similar trends but slightly underestimate the values of a_0 as well as overestimate the values of r by less than 0.01 Å (see Fig. 5 in Ref. [14]). Also, our values of Sc–F–Sc angle γ (Fig. 4) are well reproduced (see Fig. S5 in Supplemental Material of Ref. [14]) within ± 3°.

IV. COMPUTATIONAL DETAILS

The main EXAFS results reported in Fig. 4 are in good agreement with the previous statement for the materials with NTE, i.e., positive nearest-neighbors bond expansion and anisotropy of atom vibrations [8,18]. As we have mentioned previously, in the framework of the QHA model for NTE of ScF_3 it is impossible to explain a monotonic increase of the nearest-neighbors bond Sc–F if the Sc–F–Sc angles are rigid.

The simplest way to take into account the NTE and the EXAFS data with a monotonic increase of the nearest-neighbor bonds Sc–F and a decrease of the Sc–F–Sc angles is to apply a model based on the deformation of the cubic structure [$Pm\bar{3}m$(221) space group] through fluorine atom displacements described, for example, by the $Im\bar{3}$(204) space group. Obviously, this is a technical approach to mimic the local dynamic fluctuations in the ScF_3 structure. With this approach, we overcome the limits of the quasiharmonic approximation as far as the effects of large atomic vibrations of F atoms perpendicular to the chain Sc–F–Sc are introduced into the *ab initio* QHA calculations on the basis of experimental data.

In both $Pm\bar{3}m$(221) and $Im\bar{3}$(204) structures, the lattice parameter contraction is taken from the experimental diffraction data [6], whereas in the $Im\bar{3}$(204) model fluorine atoms placed at 24g Wyckoff position are allowed additionally to displace in the direction perpendicular to the Sc–F–Sc chains, as predicted by the average elongation of the Sc–F bond measured by EXAFS, thus simulating octahedra tilting on thermal

librations (see Fig. 1 and Table I in Supplemental Material [30]). Technically, we used a large supercell ($2a_0 \times 2a_0 \times 2a_0$) consisting of 32 atoms, which was also taken to describe the ScF_3 electronic structure and infrared spectra at elevated temperatures.

Regular [space group $Pm\bar{3}m(221)$] and fluorine-displaced [space group $Im\bar{3}(204)$] cubic ScF_3 crystals were simulated by means of linear combination of atomic orbitals (LCAO) within the framework of the hybrid DFT/HF approach.

In order to perform hybrid LCAO calculations, we used the CRYSTAL14 code [31,32], which employs Gaussian-type functions centered on atomic nuclei as the basis sets. The triple-ζ all-valence basis sets with polarization functions as suggested in Ref. [33] were used for both fluorine and scandium atoms. The revised version of the PBE0 hybrid exchange-correlation DFT/HF functional with 33.3% of Hartree-Fock exchange [34] was employed. The chosen exchange-correlation functional yields the lattice parameter $a_0 = 4.0257$ Å, which is in excellent agreement with its experimental value of 4.026 Å at $T = 0$ K [6]. This result is important for a correct description of very small lattice parameter variation in ScF_3 upon NTE effect. The choice of the hybrid functional was additionally justified by calculating the band gap (E_g). The precise experimental value of the band gap of ScF_3 is not known, but it is estimated to be larger than 7–8 eV [11]. Our results based on the hybrid exchange-correlation functionals within the DFT/HF–LCAO method indicate that the cubic ScF_3 is a wide-band-gap insulator with $E_g = 10.54$ eV, with good agreement with the experimental estimation of E_g in Ref. [11].

To provide the balanced summation over the direct and reciprocal lattices of ScF_3, the reciprocal space integration was performed by sampling the BZ with the $8 \times 8 \times 8$ Pack-Monkhorst k mesh [35] that results in 35 evenly distributed k points in the irreducible BZ. Calculations are considered as converged only when the total energy differs by less than 10^{-9} a.u. in two successive cycles of the self-consistency procedure. Threshold parameters for evaluation of different types of bielectronic integrals, such as overlap and penetration tolerances for Coulomb integrals, overlap tolerance for exchange integrals, and pseudo-overlap tolerances for exchange integral series [31] were set to 10^{-8}, 10^{-8}, 10^{-8}, 10^{-8}, and 10^{-16}, respectively [31]. Effective charges on atoms were estimated using Mulliken population analysis [31,36].

The details of the electronic structure calculations are provided in Supplemental Material [30]. The use of the revised version of hybrid exchange-correlation DFT/HF functional PBE0 [34] allowed us to reproduce accurately the experimental values of the lattice constant and the band gap of ScF_3 [30]. Also, the calculated occupied and empty projected density of F $2p$ states (PDOS) are in agreement with the experimentally measured valence-band photoelectron spectrum [37] and the F $1s$ x-ray absorption spectrum [11], respectively [30]. These results support the good reliability of our lattice dynamics simulations.

The phonon frequencies at the symmetry points of BZ were calculated here in harmonic approximation by the frozen phonon method [2]. In this direct method, the phonon frequencies are calculated from forces generated by small atomic displacements from equilibrium positions in a supercell. The used $2a_0 \times 2a_0 \times 2a_0$ supercell allowed us to calculate the frequencies at the BZ symmetry points Γ, R, M, and X [38].

The phonon dispersion was calculated by means of supercell approach according to the prescription given in CRYSTAL14 code [31]. The nonanalytical part was obtained with a finite field supercell approach for the high-frequency dielectric constant and a Wannier function scheme for the evaluation of Born charges (for details see Ref. [31] and references therein). The isotropic diagonal dielectric tensor components for the calculation of the LO/TO splitting were evaluated at the supercell size of $6a_0 \times 6a_0 \times 6a_0$. The calculated dielectric constant ϵ is equal to 1.84, which is close to $\epsilon \simeq 2$, evaluated from the value of refractive index n obtained experimentally in Ref. [39]. These results were used to calculate the IR spectra of ScF_3 from a complex dielectric function using a raw superposition of Gaussian peaks with the full width at half maximum set to 5 cm^{-1} [31].

V. RESULTS AND DISCUSSION

A. Phonon structure

Table I shows the phonon mode symmetry in a ScF_3 crystal [the symmetry space group $221(O_h^1)$]. In principle, two equivalent descriptions of ScF_3 structure can be given: $1a$(Sc)$3d$(F) and $1b$(Sc)$3c$(F). The first structure description is taken here.

The phonon modes symmetry is given for the symmetry points of simple cubic lattice Brillouin zone. For the space group irreps the labels from Ref. [40] are used. The phonon symmetry is found using the site-symmetry approach [41], which establishes symmetry relations between the localized states (in particular, local atomic displacements) and crystal extended states (phonons) and is realized in the computer code SITESYMM at http://www.cryst.ehu.es/ (Bilbao Crystallographic Server).

Figure 5 shows the calculated phonon dispersions along high-symmetry BZ directions Γ-X-M-R-Γ (left panel) as well as the total and partial phonon density of states (right panel). The calculated total phonon DOS is compared to experimental neutron-weighted phonon DOS at 7 K (red dotted line) from Ref. [4] (right panel): The two curves are in good qualitative agreement. Note that our results are also in agreement with the previous *ab initio* calculations [4,42].

TABLE I. Phonon symmetry in a ScF_3 crystal [space group $Pm\bar{3}m(221)$].

		$\Gamma(0, 0, 0)$	$R(1/2, 1/2, 1/2)$	$M(1/2, 1/2, 0)$	$X(1/2, 0, 0)$
$1a(O_h)$:	$t_{1u}(x,y,z)$	4^-	4^-	$3^-\ 5^-$	$3^-\ 5^-$
$3d(D_{4h})$:	$a_{2u}(z)$	4^-	$1^+\ 3^+$	$1^+\ 2^+\ 3^-$	$1^+\ 5^-$
	$e_u(x,y)$	$4^-\ 5^-$	$4^+\ 5^+$	$3^+\ 4^+\ 5^+\ 5^-$	$3^-\ 4^-\ 5^-\ 5^+$

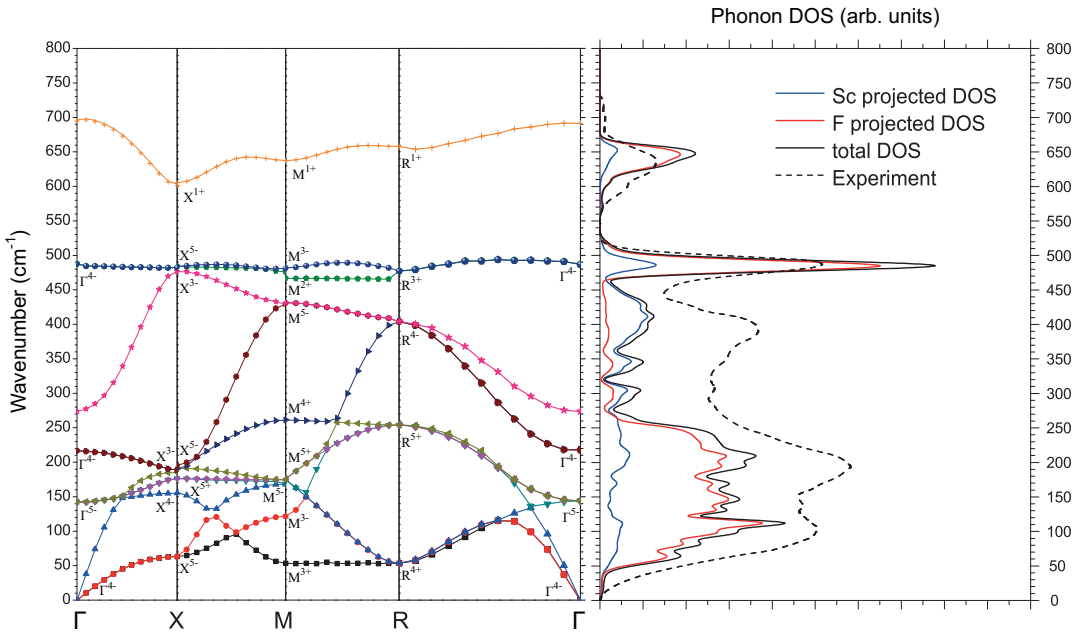

FIG. 5. Calculated phonon dispersions for ScF_3 in $Pm\bar{3}m(221)$ phase along high-symmetry BZ directions Γ-*X*-*M*-*R*-Γ (left panel). Total and partial phonon density of states (DOS) obtained from dispersion curves (solid lines) are compared to experimental neutron-weighted phonon DOS at 7 K (black dashed line) adapted from Ref. [4] (right panel).

Table II shows the phonon frequencies at the symmetry points of BZ. It is seen that the two phonon modes with the smallest frequencies 52.3 cm^{-1} and 52.7 cm^{-1} have the symmetry R^{4+} and M^{3+}, respectively, and are related to the F atom displacements. This result agrees with that of force-field calculations [13], where abnormally low frequencies were found for the weak dispersion *R*-*M* branch between triply degenerate *R* and nondegenerate *M* modes, in which fluorine atoms are displaced. The domination of F atoms in the lower-energy parts of phonon DOS was also found in planewave local density approximation (LDA) calculations [4]. For the low-energy *R* and *M* modes anomalous negative Grüneisen constants were found in Ref. [4].

As it is seen from Table I, the phonon modes R^{4+} and M^{3+} consist of strictly transversal displacements of the F atom. This means that any structure distortion (temperature or pressure change) can produce the corresponding displacements of F atoms and generate displacive phase transition. The isotropy subgroup group-theoretical approach [43] allows us to connect the second-order displacive phase transitions in crystals with the symmetry of softening phonon modes. For the phonons with symmetry R^{4+} and M^{3+} (space group O_h^1) the isotropy subgroups $R\bar{3}c(167)$ and $Im\bar{3}(204)$, respectively, can be obtained by the group-theoretical analysis using the isotropy subgroup approach. Meanwhile, the subgroup $R\bar{3}c(167)$ was found for ScF_3 crystal above 0.6 GPa in the pressure-induced phase transition study using synchrotron radiation diffraction, polarization microscopy, and Raman spectroscopy in Ref. [44]. The subgroup $Im\bar{3}(204)$ was found for ReO_3 crystal in a high-pressure neutron powder diffraction study [45].

In the next section we use the model based on the space group $Im\bar{3}(204)$ and a set of structural parameters reported in Table I in Supplemental Material [30] to explain the behavior of the IR spectra in ScF_3 due to the NTE effect. The model is connected in ScF_3 with M^{3+}-phonon softening and allows us to technically mimic dynamic fluctuations in the cubic ScF_3 structure.

TABLE II. Phonon frequencies (cm^{-1}) in a ScF_3 crystal [space group $Pm\bar{3}m(221)$].

Γ(0, 0, 0)	*R*(1/2, 1/2, 1/2)	*M*(1/2, 1/2, 0)	*X*(1/2, 0, 0)
4^- 0.0	4^+ 52.3	3^+ 52.7	5^- 63.3
5^- 143.4	5^+ 253.8	3^- 121.7	4^- 155.7
4^- 217.5	4^- 403.6	5^- 168.7	5^+ 176.0
4^- 486.8	3^+ 474.9	5^+ 174.3	3^- 185.6
	1^+ 655.1	4^+ 260.7	5^- 191.4
		5^- 429.1	3^- 476.9
		2^+ 475.8	5^- 484.1
		3^- 481.7	1^+ 597.4
		1^+ 630.2	

B. Infrared absorption spectra

Temperature dependence (6–300 K) of the experimental infrared absorption spectra of ScF_3 is shown in Fig. 2. Two bands at 220 and 520 cm^{-1} are visible in the wave-number range of 150–650 cm^{-1}. They correspond respectively to the F–Sc–F bending and Sc–F stretching Γ^{4-} modes (Table II). As temperature increases from 6 to 300 K, each of these bands shifts by about ~6 cm^{-1} toward the other. Such behavior is consistent with that observed for the same vibrational modes in temperature-dependent inelastic-neutron-scattering experiments in Ref. [4].

To understand the temperature dependence of two bands, we have calculated infrared absorption spectra as described in Sec. IV for two models constructed for $Pm\bar{3}m(221)$ and

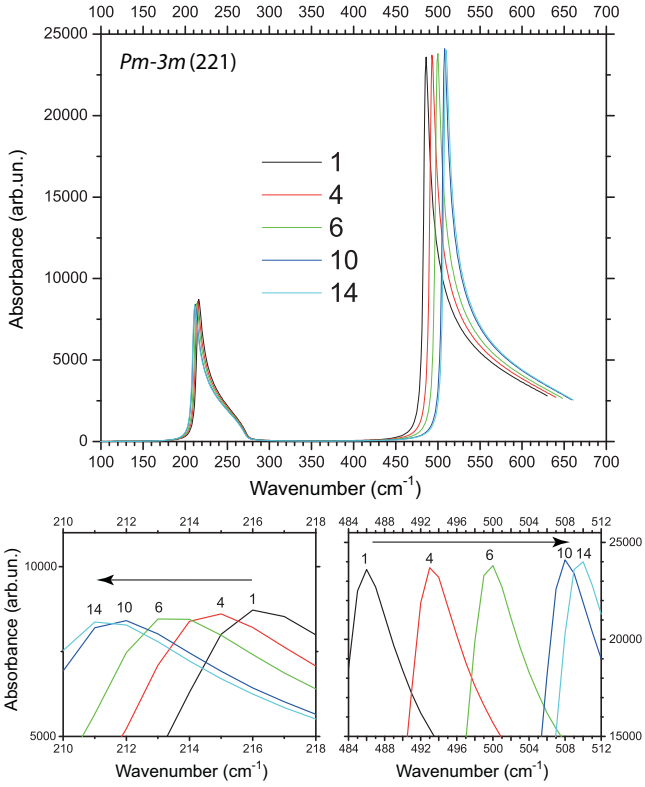

FIG. 6. Calculated infrared absorption spectra of ScF_3 in $Pm\bar{3}m$ phase for selected values of contracting lattice parameter a_0. Curves are numbered according to Table I in Supplemental Material [30]. Increasing numbers correspond to higher temperature T and shorter a_0, as also shown in Fig. 8.

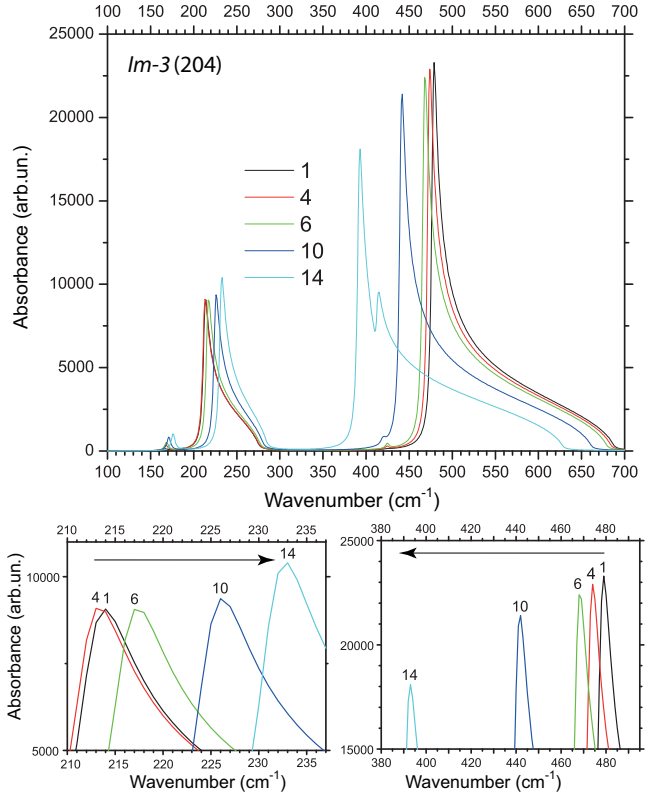

FIG. 7. Calculated infrared absorption spectra of ScF_3 in $Im\bar{3}$ phase for selected values of contracting lattice parameter a_0 and fluorine atoms displacements. Curves are numbered according to Table I in Supplemental Material [30]. Increasing numbers correspond to higher temperature T and shorter a_0, as also shown in Fig. 8.

$Im\bar{3}(204)$ space groups. Note that the Sc–F–Sc angle $\gamma = 180^\circ$ and $r_{Sc-F} = a_0/2$ in the $Pm\bar{3}m(221)$ model, whereas the ScF_6 octahedra are tilted in the $Im\bar{3}(204)$ model in such a way that the Sc–F–Sc angle $\gamma < 180^\circ$ and the distance $r_{Sc-F} > a_0/2$ (see Table I in Supplemental Material [30]). The simulated IR spectra, including the LO-TO splitting, are shown in Figs. 6 and 7 for the values of lattice parameter a_0 corresponding to the temperature interval from 10 to 1100 K. The temperature dependencies of the IR-active TO phonon modes, contributing to the two bands, are also presented separately in Fig. 8.

In general, the shift of the mode frequency is determined by the lattice parameter variation (in terms of Grüneisen parameter) and by the anharmonic phonon-phonon coupling [46].

As one can see, the results for the $Pm\bar{3}m(221)$ model predict frequency change of both modes (Fig. 6) in the direction opposite to that observed experimentally (Fig. 2). Upon temperature increase in the range from 10 to 300 K, the lattice contraction leads to a decrease in the bending mode frequency by $\sim$2.5 cm^{-1}, whereas the stretching mode frequency increases significantly by $\sim$14 cm^{-1}. Note that this behavior continues on further lattice contraction. Thus the calculations for ScF_3 based on the crystallographic space group and quasiharmonic approximation are not able to reproduce the experimentally observed behavior of IR absorption spectra.

In the $Im\bar{3}(204)$ model, simulating tilting of ScF_6 octahedra and expansion of the Sc-F bonds, the qualitative behavior of both infrared modes (Figs. 7 and 8) follows that observed experimentally (Fig. 2). In particular, in the temperature range

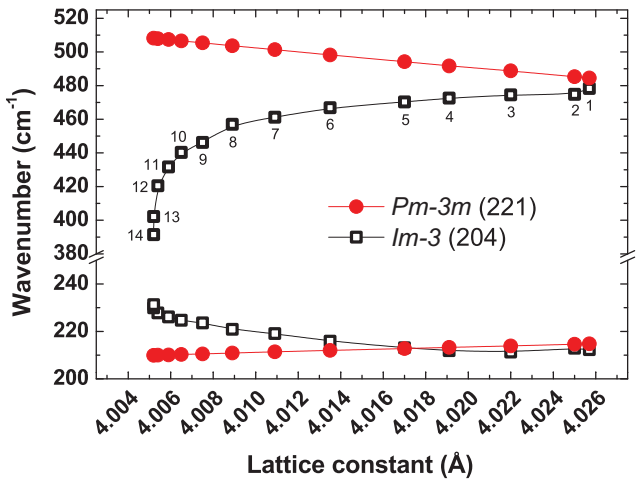

FIG. 8. Variation of the frequencies for IR-active TO phonon modes in ScF_3 as a function of the lattice parameter in $Pm\bar{3}m(221)$ and $Im\bar{3}(204)$ phases. Points are numbered according to Table I in Supplemental Material [30].

from 10 to 300 K, the bending mode frequency increases by $\sim$4 cm^{-1}, whereas the stretching mode frequency decreases by $\sim$12 cm^{-1}. Thus this model allows us to go beyond the quasiharmonic approximation and is able to reproduce qualitatively the experimental IR data for ScF_3 on negative thermal expansion; however, its simplicity limits the quantitative accuracy (which is still remarkable). Note that the observed behavior continues on lattice contraction, leading to the largest expected shifts for the F–Sc–F bending and Sc–F stretching bands of about +20 cm^{-1} and −90 cm^{-1} at 1100 K. The confirmation of our prediction of the IR spectra behavior in ScF_3 at high temperatures above 300 K is waiting for future experimental studies.

VI. CONCLUSIONS

The influence of the negative thermal expansion on the temperature dependence (10–300 K) of infrared absorption spectra of cubic ScF_3 was studied using *ab initio* lattice dynamics simulations within the quasiharmonic approximation but overcoming its limits by imposing a change of local structure that was able to simulate the effects of large transverse vibrations of F atoms.

We showed that the atomic and electronic structure of ScF_3 are well reproduced by a hybrid DFT/HF–LCAO method. In particular, the calculated lattice parameter $a_0 = 4.0257$ Å is in excellent agreement with its experimental value at $T = 0$ K, and the band gap $E_g = 10.54$ eV agrees well with the expected value [11]. A deviation of ionic charges from the formal ones points to the partial covalent nature of the Sc–F bonds in ScF_3. Calculated partial density of electron states is in good agreement with valence-band photoelectron [37] and the F 1*s* x-ray absorption [11] spectra. These results support reliability of our lattice dynamics calculations.

We found that the total density of phonon states determined within quasiharmonic approximation from phonon dispersion curves, calculated along the high-symmetry directions Γ-*X*-*M*-*R*-Γ of the Brillouin zone, agrees reasonably well with the experimental neutron-weighted phonon DOS measured at 7 K in Ref. [4].

At the same time, the temperature dependence of the experimentally measured IR absorption spectra, consisting of two bands at 220 and 520 cm^{-1} due to the F–Sc–F bending and Sc–F stretching Γ^{4-} modes, cannot be explained within the quasiharmonic approximation, which predicts shifts of these bands in an opposite direction with respect to that experimentally observed.

To resolve this issue, we have developed a simple model which accounts both for negative lattice thermal expansion and for Sc–F bond length elongation. Our model is based on the symmetry analysis of phonon modes and uses as input the temperature-dependent experimental results of diffraction [6] and EXAFS studies. This model, overcoming the limits of standard use of quasiharmonic approximation, allows us to reproduce the unexpected experimental behavior observed for two bands in the IR absorption spectrum of ScF_3 and can be also applied for the interpretation of its other spectroscopic properties [47].

ACKNOWLEDGMENTS

The authors are greatly indebted to D. Gryaznov, V. Kashcheyevs, M. Krack, V. Pankratov, A. I. Popov, L. Shirmane, and Yu. F. Zhukovskii for many stimulating discussions. R.A.E. thanks St. Petersburg State University Computer Center for assistance in the accomplishment of high-performance computations. S.E.A. thanks the Department of Physics, University of Trento (Italy), and FBK–Fondazione Bruno Kessler (Trento, Italy) for scientific and economical support during and after his Ph.D. thesis. The authors thank the staff of the AILES beamline at SOLEIL synchrotron for providing the opportunity to perform the infrared experiment. We also gratefully acknowledge the assistance of Giuliana Aquilanti and of the staff members of the ELETTRA XAFS beamline during the EXAFS experiment performed within Proposal No. 20120215. The work was partially supported by the Latvian Science Council Grants No. 402/2012 (J.P.) and No. 187/2012 (A.K.).

[1] B. Fultz, Progr. Mater. Sci. **55**, 247 (2010).
[2] K. Parlinski, Z. Q. Li, and Y. Kawazoe, Phys. Rev. Lett. **78**, 4063 (1997).
[3] A. Glensk, B. Grabowski, T. Hickel, and J. Neugebauer, Phys. Rev. Lett. **114**, 195901 (2015).
[4] C. W. Li, X. Tang, J. A. Muñoz, J. B. Keith, S. J. Tracy, D. L. Abernathy, and B. Fultz, Phys. Rev. Lett. **107**, 195504 (2011).
[5] T. Lan, C. W. Li, O. Hellman, D. S. Kim, J. A. Muñoz, H. Smith, D. L. Abernathy, and B. Fultz, Phys. Rev. B **92**, 054304 (2015).
[6] B. K. Greve, K. L. Martin, P. L. Lee, P. J. Chupas, K. W. Chapman, and A. P. Wilkinson, J. Am. Chem. Soc. **132**, 15496 (2010).
[7] T. Chatterji, P. F. Henry, R. Mittal, and S. L. Chaplot, Phys. Rev. B **78**, 134105 (2008).
[8] J. Purans, P. Fornasini, S. E. Ali, G. Dalba, A. Kuzmin, and F. Rocca, Phys. Rev. B **92**, 014302 (2015).
[9] S. U. Handunkanda, E. B. Curry, V. Voronov, A. H. Said, G. G. Guzmán-Verri, R. T. Brierley, P. B. Littlewood, and J. N. Hancock, Phys. Rev. B **92**, 134101 (2015).
[10] E. E. Rodriguez, A. Llobet, T. Proffen, B. C. Melot, R. Seshadri, P. B. Littlewood, and A. K. Cheetham, J. Appl. Phys. **105**, 114901 (2009).
[11] M. Umeda, Y. Tezuka, S. Shin, and A. Yagishita, Phys. Rev. B **53**, 1783 (1996).
[12] K. Aleksandrov, N. Voronov, A. Vtyurin, A. Krylov, M. Molokeev, A. Oreshonkov, S. Goryainov, A. Likhacheva, and A. Ancharov, Phys. Solid State **53**, 564 (2011).
[13] K. Aleksandrov, V. Voronov, A. Vtyurin, S. Goryainov, N. Zamkova, V. Zinenko, and A. Krylov, J. Exper. Theor. Phys. **94**, 977 (2002).
[14] P. Lazar, T. Bučko, and J. Hafner, Phys. Rev. B **92**, 224302 (2015).

[15] T. Lan, C. W. Li, J. L. Niedziela, H. Smith, D. L. Abernathy, G. R. Rossman, and B. Fultz, Phys. Rev. B **89**, 054306 (2014).
[16] D. Marx and M. Parrinello, J. Chem. Phys. **104**, 4077 (1996).
[17] P. Fornasini and R. Grisenti, J. Synchrotron Rad. **22**, 1242 (2015).
[18] S. a Beccara, G. Dalba, P. Fornasini, R. Grisenti, A. Sanson, and F. Rocca, Phys. Rev. Lett. **89**, 025503 (2002).
[19] P. Roy, M. Rouzires, Z. Qi, and O. Chubar, Infrared Phys. Techn. **49**, 139 (2006).
[20] A. Di Cicco, G. Aquilanti, M. Minicucci, E. Principi, N. Novello, A. Cognigni, and L. Olivi, J. Phys.: Conf. Ser. **190**, 012043 (2009).
[21] L. Hu, J. Chen, L. Fan, Y. Ren, Y. Rong, Z. Pan, J. Deng, R. Yu, and X. Xing, J. Am. Chem. Soc. **136**, 13566 (2014).
[22] G. Dalba, P. Fornasini, R. Grisenti, and J. Purans, Phys. Rev. Lett. **82**, 4240 (1999).
[23] A. Sanson, F. Rocca, G. Dalba, P. Fornasini, R. Grisenti, M. Dapiaggi, and G. Artioli, Phys. Rev. B **73**, 214305 (2006).
[24] W. R. Busing and H. A. Levy, Acta Crystallogr. **17**, 142 (1964).
[25] P. Fornasini, J. Phys. Condens. Matter **13**, 7859 (2001).
[26] P. Fornasini, S. a Beccara, G. Dalba, R. Grisenti, A. Sanson, M. Vaccari, and F. Rocca, Phys. Rev. B **70**, 174301 (2004).
[27] A. Kuzmin, Physica B **208-209**, 175 (1995).
[28] V. Aksenov, M. Kovalchuk, A. Kuzmin, Y. Purans, and S. Tyutyunnikov, Crystallogr. Rep. **51**, 908 (2006).
[29] A. Kuzmin and J. Chaboy, IUCrJ **1**, 571 (2014).
[30] See Supplemental Material at http://link.aps.org/supplemental/10.1103/PhysRevB.93.214101 for a description of the starting structural model and calculation results on the electronic structure of ScF_3.
[31] R. Dovesi, V. R. Saunders, C. Roetti, R. Orlando, C. M. Zicovich-Wilson, F. Pascale, B. Civalleri, K. Doll, N. M. Harrison, I. J. Bush, P. D'Arco, M. Llunell, M. Causá, and Y. Noël, *CRYSTAL14 User's Manual* (University of Torino, Torino, 2014).
[32] R. Dovesi, R. Orlando, A. Erba, C. Zicovich-Wilson, B. Civalleri, S. Casassa, L. Maschio, M. Ferrabone, M. De La Pierre, P. D'Arco, Y. Nol, M. Caus, M. Rrat, and B. Kirtman, Int. J. Quantum Chem. **114**, 1287 (2014).
[33] M. F. Peintinger, D. V. Oliveira, and T. Bredow, J. Comp. Chem. **34**, 451 (2013).
[34] C. A. Guido, E. Brémond, C. Adamo, and P. Cortona, J. Chem. Phys. **138**, 021104 (2013).
[35] H. J. Monkhorst and J. D. Pack, Phys. Rev. B **13**, 5188 (1976).
[36] R. S. Mulliken, J. Chem. Phys. **23**, 1833 (1955).
[37] S. Shin, Y. Tezuka, T. Ishii, and Y. Ueda, Solid State Commun. **87**, 1051 (1993).
[38] R. A. Evarestov and M. V. Losev, J. Comp. Chem. **30**, 2645 (2009).
[39] P. Chindaudom and K. Vedam, Appl. Opt. **33**, 2664 (1994).
[40] A. P. Cracknell, B. Davies, S. C. Miller, and W. F. Love, *Kronecker Product Tables. Vol. 1. General Introduction and Tables of Irreducible Representations of Space Groups* (IFI/Plenum, New York, 1979).
[41] R. A. Evarestov and V. P. Smirnov, *Site Symmetry in Crystals: Theory and Applications*, 2nd ed., Springer Series in Solid-State Sciences, Vol. 153 (Springer-Verlag, Berlin, 1997).
[42] Y. Liu, Z. Wang, M. Wu, Q. Sun, M. Chao, and Y. Jia, Comp. Mater. Sci. **107**, 157 (2015).
[43] H. T. Stokes and D. M. Hatch, *Isotropy Subgroups of the 230 Crystallographic Space Groups* (World Scientific, Singapore, 1988).
[44] K. Aleksandrov, V. Voronov, A. Vtyurin, A. Krylov, M. Molokeev, M. Pavlovskii, S. Goryainov, A. Likhacheva, and A. Ancharov, Phys. Solid State **51**, 810 (2009).
[45] J.-E. Jørgensen, W. G. Marshall, R. I. Smith, J. Staun Olsen, and L. Gerward, J. Appl. Cryst. **37**, 857 (2004).
[46] J. R. Jasperse, A. Kahan, J. N. Plendl, and S. S. Mitra, Phys. Rev. **146**, 526 (1966).
[47] A. Antuzevics, U. Rogulis, A. Fedotovs, D. Berzins, V. N. Voronov, and J. Purans, Phys. Scr. **90**, 115801 (2015).